Das et al. Earth, Planets and Space (2016) 68:11
DOI 10.1186/s40623-016-0381-9

Earth, Planets and Space
a SpringerOpen Journal

FULL PAPER Open Access

$^{40}Ar/^{39}Ar$ and cosmic ray exposure ages of plagioclase-rich lithic fragments from Apollo 17 regolith, 78461

J. P. Das[1*], S. L. Baldwin[1] and J. W. Delano[2]

Abstract

Argon isotopic data is used to assess the potential of low-mass samples collected by sample return missions on planetary objects (e.g., Moon, Mars, asteroids), to reveal planetary surface processes. We report the first $^{40}Ar/^{39}Ar$ ages and ^{38}Ar cosmic ray exposure (CRE) ages, determined for eleven submillimeter-sized (ranging from 0.06 to 1.2 mg) plagioclase-rich lithic fragments from Apollo 17 regolith sample 78461 collected at the base of the Sculptured Hills. Total fusion analysis was used to outgas argon from the lithic fragments. Three different approaches were used to determine $^{40}Ar/^{39}Ar$ ages and illustrate the sensitivity of age determination to the choice of trapped $(^{40}Ar/^{36}Ar)_t$. $^{40}Ar/^{39}Ar$ ages range from ~4.0 to 4.4 Ga with one exception (Plag#10). Surface CRE ages, based on ^{38}Ar, range from ~1 to 24 Ma. The relatively young CRE ages suggest recent re-working of the upper few centimeters of the regolith. The CRE ages may result from the effect of downslope movement of materials to the base of the Sculptured Hills from higher elevations. The apparent $^{40}Ar/^{39}Ar$ age for Plag#10 is >5 Ga and yielded the oldest CRE age (i.e., ~24 Ma). We interpret this data to indicate the presence of parentless ^{40}Ar in Plag#10, originating in the lunar atmosphere and implanted in lunar regolith by solar wind. Based on a chemical mixing model, plagioclase compositions, and $^{40}Ar/^{39}Ar$ ages, we conclude that lithic fragments originated from Mg-suite of highland rocks, and none were derived from the mare region.

Keywords: Lunar regolith, $^{40}Ar/^{39}Ar$ ages, ^{38}Ar cosmic ray exposure ages, Apollo 17, Planetary surfaces, Parentless ^{40}Ar

Introduction

The regolith of planetary objects (e.g., Moon, Mars, and asteroids) can be defined as the boundary layer between the solid crust and outer space. The regolith evolution on planetary objects is a function of the continuous flux of impactors of various sizes, volcanism, as well as the constant bombardment by solar and galactic energetic particles. Regolith generally consists of fragmental and unconsolidated rock material. The hyper-velocity of the impacts and the continuous bombardment of energetic particles and micrometeorites reduce the initially rocky planetary surface to increasingly finer grain-sized regolith. For example, on the lunar surface, the mean grain size of lunar regolith ranges from 40 to 800 μm and averages between 60 and 80 μm (Lucey et al. 2006). A record of impact events and interactions with cosmic rays preserved in lunar regolith can be understood by geochemical and chronological studies of lunar regolith samples. The outcome of these studies provide constraints to understand the evolution of the Earth-Moon system and inner solar system (e.g., Lucey et al. 2006; Stöffler et al. 2006). The geochemical and chronological constraints developed based on lunar regolith studies can be applied to the surfaces of other solar system objects and used as a guide for future and ongoing missions like Hayabusa (Tsuda et al. 2013; Okada et al. 2015) to a C-type asteroid 1999 JU3, OSIRIS-REx sample return mission (Lauretta and Team 2012) to the asteroid 101955 Bennu, and the Mars Science Laboratory (Grotzinger et al. 2012), currently conducting experiments on the Martian surface. Kring (2015) describes how the success of NASA's Orion crew vehicle, as well as the outcome of current lunar orbiters, has revitalized future interest in robotic and human exploration programs to the moon and beyond.

* Correspondence: jdas@syr.edu
[1]Department of Earth Sciences, Syracuse University, Syracuse, NY 13244, USA
Full list of author information is available at the end of the article

Regolith sample collected at station 8, Apollo 17

The Apollo 17 landing site is located in the center of the Taurus-Littrow valley. One of the prominent geological features of the valley is the highland unit found near the north massif, the Sculptured Hills. Apollo 17 astronauts sampled the regolith at the base of the Sculptured Hills during their last surface traverse at station 8 (latitude 20.278° N, longitude 30.848° S; Robinson and Jolliff 2002). They dug a 25-cm-deep trench (Wolfe et al. 1981) that revealed the best preserved lunar regolith stratigraphy collected during the Apollo missions (Mitchell et al. 1973; Fig. 1). Based on the chemical composition of the deepest layer of the trench (i.e., sample 78421), Korotev and Kremser (1992) concluded that the regolith represents six chemical components. Among them, three chemical components are of mare origin: (1) high-Ti (HT) mare basalt, (2) very-low-Ti (VLT) basalt, and (3) pyroclastic orange glass. The other three chemical components are of highland origin: (4) impact-melt noritic breccia (NB), (5) anorthositic norite (AN) breccia, and (6) Mg-suite (high Mg/Fe troctolites and norites). A similar study by Simon et al. (1981) found that mare volcanics and highland-derived fragments were present in equal proportions in Apollo 17 regolith sample 78221. A mixing model based on the major and trace-element composition of the sample from the top layer of trench regolith (i.e., 78481) suggest mixing of 40–50 % mare and 52–59 % highland components (Rhodes et al. 1974). Goswami and Lal (1974) performed nuclear track studies on the samples from the trench and observed that the density of tracks observed in the bottom sample (i.e., 78121) is only slightly less than the track density observed in the surface sample (i.e., 78481) and concluded that the track density distribution pattern, along with the knowledge of the geological setting at station 8, can be used to characterize the macroscopic lunar surface transport processes including regolith mixing and down slope movement. Prior to our study, the crystallization and metamorphic ages on this trench regolith sample were unknown (Meyer 2010). We present the first $^{40}Ar/^{39}Ar$ ages and ^{38}Ar cosmic ray exposure (CRE) ages on plagioclase-rich lithic fragments separated from the 78461 trench regolith sample collected at station 8.

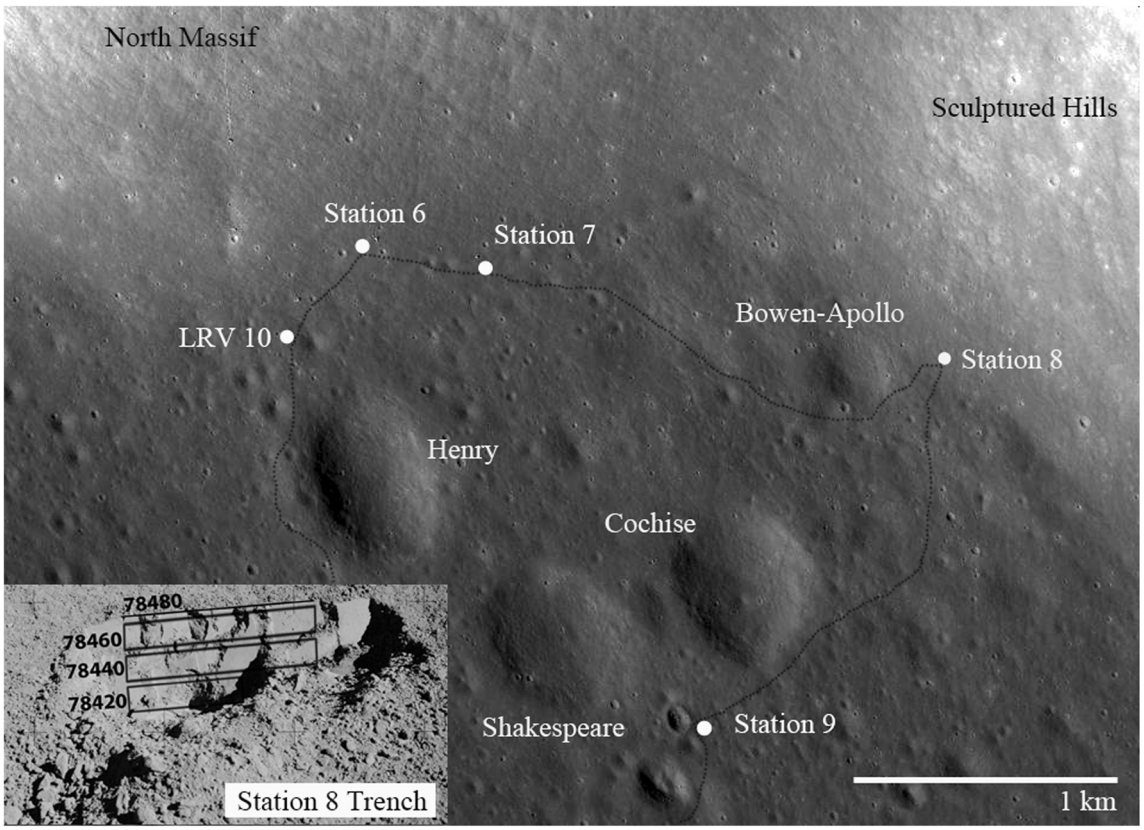

Fig. 1 Topographic image of the Sculptured Hills and an inset image of station 8 trench. The moderately inclined transition zone between the Sculptured Hills and the Taurus-Littrow Valley floor with Apollo 17 mission traverses indicated. Station 8 was located at the base of the Sculptured Hills. A 25-cm-deep trench (shown in *inset*) was sampled at station 8. The plagioclase-rich lithic fragments analyzed in this work were separated from 78460 (1 to 6 cm layer). Also, the crew climbed up towards the hills to sample the 0.5-m boulder (i.e., 78235). Background image: LRO Narrow Angle Camera (NAC) high-resolution image (0.5 m per pixel) laid over the wide-angle Camera morphologic basemap (100 m/pixel). *Inset image source*: Lunar and Planetary Institute, Houston (http://www.lpi.usra.edu/resources/apollo/frame/?AS17-142-21720)

These chronology data are used together with plagioclase compositions and a mixing model to determine the origin and duration that the regolith resided on the lunar surface.

Sample and experimental details

Sample details

Regolith sample 78460 was collected at a depth interval of 1–6 cm at station 8 at the base of the Sculptured Hills (Meyer 2010), and ~20 m above the Taurus-Littrow valley floor from the Apollo 17 landing site (Fig. 1). Plagioclase-rich lithic fragments comprise ~7–9 modal percentage of the 1000–90 μm (Heiken and McKay 1974) size fractions of station 8 regolith samples. The median grain size of regolith sample 78460 is 47 μm (Graf 1993). The eleven plagioclase-rich lithic fragments analyzed in this study were handpicked from the 1000–90-μm fraction of a 5-g aliquot of 78461, which is the <1 mm size fraction of 78460 (Butler 1973). The sieved fraction was ultrasonically cleaned in acetone, dried, handpicked, and weighed. Out of eleven handpicked lithic fragments, eight fragments were less than 0.52 mg. The other three fragments, Plag#21, Plag#23, and Plag#24 weighed 1.20, 1.08, and 0.72 mg, respectively (Table 1).

Chemical characterization of plagioclase-rich lithic fragments

Plagioclase-rich fragments were individually mounted in CrystalBond© adhesive, ground, polished, and carbon coated. Samples were analyzed for major element composition using a CAMECA SX-100 electron microprobe at Rensselaer Polytechnic Institute with run condition of 15 kV, 20 nA, and 30-s counting times with a 10-μm-diameter beam. Samples were subsequently polished with 0.3-μm alumina powder to remove the carbon coating and warmed to ~100 °C for ~1 min to soften the CrystalBond© adhesive for removal of each lithic fragment. These were then ultrasonically cleaned in acetone to remove adhering CrystalBond©. Major elemental compositions of the eleven plagioclase-rich lithic fragments are given in Table 1. The lithic fragments contain Ca-rich feldspar (i.e., anorthite), with compositions ranging from An_{93} to An_{96} (Table 1). The K_2O contents range from 0.03 to 0.28 wt.% suggesting 200 to 2300 ppm of K in the fragments. The Fe/(Fe + Mg) ratio varies from 0.19 (Plag#1) to 0.84 (Plag#24). Given the size of the plagioclase lithic fragments (<48 μm), we were unable to obtain a pure plagioclase separate using standard mineral separation techniques.

Irradiation of plagioclase-rich lithic fragments

Following electron probe analysis, each plagioclase-rich lithic fragment was individually packed in Al foil and irradiated for 100 h in the cadmium-lined in-core irradiation tube (CLICIT) facility of the TRIGA reactor at Oregon State University, USA. Cadmium shielding was used to minimize the production of ^{38}Ar from ^{37}Cl and undesirable isotopic interference reactions. The neutron flux was monitored using Hb3gr (hornblende, PP-20) hornblende (Turner 1971; Jourdan and Renne 2007; Schwarz and Trieloff 2007). These flux monitor standards were placed between the plagioclase-rich lithic fragments to monitor the fast neutron dose. In addition, CaF_2 and $KSiO_3$ glasses were also placed between the samples to derive correction factors for reactor-produced ^{37}Ar and ^{39}Ar.

Gas extraction and mass spectrometric measurements

Following irradiation, the plagioclase-rich lithic fragments, international standard Hb3gr (hornblende, PP-20) flux monitors, CaF_2, and $KSiO_3$ were unwrapped from Al foil. The samples were outgassed using a CO_2 laser (Synrad model J48) with beam diameter of 3.5 mm and ~8 W of power. Extracted Ar from each fused sample was measured

Table 1 Chemical composition of plagioclase-rich lithic fragments separated from Apollo 17, 78461 regolith

Sample	Weight (mg)	SiO_2 (wt.%)	TiO_2	Al_2O_3	FeO	MgO	CaO	Na_2O	K_2O	Fe/(Fe + Mg)	Σ	An(%)
Plag#1	0.22	44.34	0.00	35.68	0.01	0.05	19.25	0.53	0.10	0.19	99.96	93.6
Plag#3	0.17	44.28	0.01	36.18	0.03	0.03	18.78	0.64	0.03	0.54	99.98	94.0
Plag#6	0.06	45.01	0.00	35.97	0.04	0.05	18.20	0.62	0.10	0.48	99.99	93.6
Plag#9	0.20	44.47	0.01	35.50	0.02	0.02	19.07	0.75	0.11	0.54	99.95	92.8
Plag#10	0.16	43.98	0.01	35.97	0.08	0.07	19.40	0.55	0.03	0.57	100.09	95.0
Plag#14	0.18	44.45	0.00	35.43	0.07	0.03	19.25	0.68	0.02	0.73	99.93	94.4
Plag#21	1.20	44.29	0.01	35.90	0.05	0.08	19.02	0.59	0.05	0.42	99.99	95.0
Plag#22	0.52	44.11	0.08	34.49	0.82	0.50	19.02	0.38	0.28	0.66	99.68	96.5
Plag#23	1.08	43.25	0.01	36.16	0.21	0.07	19.86	0.37	0.05	0.78	99.98	93.2
Plag#24	0.72	44.19	0.03	35.71	0.27	0.06	18.89	0.66	0.16	0.84	99.97	95.3
Plag#25	0.45	43.78	0.04	35.52	0.35	0.21	19.53	0.48	0.07	0.66	99.98	95.3

Values of major element oxides are average of three analyses. Percentage fraction of anorthite in plagioclase feldspar is indicated (An%)

using a VG5400 noble gas mass spectrometer in Syracuse University's Noble Gas Isotope Research Laboratory. Based on the measurement of 8 PP-20 grains (1073.6 ± 4.6 (1σ); Schwarz and Trieloff (2007)), the mean J value for the samples is calculated to be 0.02643 ± 0.00021 (1σ). These values are similar to those reported for 100 h irradiation at the CLICIT facility (Fernandes et al. 2013; Gombosi et al. 2015). The correction factors for reactor-produced isotopes are as follows: $(^{39}Ar/^{37}Ar)_{Ca} = (7.57 \pm 0.34) \times 10^{-4}$, $(^{36}Ar/^{37}Ar)_{Ca} = (3.22 \pm 1.26) \times 10^{-4}$, and $(^{40}Ar/^{39}Ar)_{K} = 0.01576 \pm 0.0004$. After extraction, reactive gases were removed using SAES ST-707 getters. The purified gas was then expanded into the VG5400 mass spectrometer, and 11 cycles at m/e = 40, 39, 38, 37, 36, and 35 were measured in peak jumping mode. Blank measurements were performed before and after every sample analysis to determine the background for Ar isotopes in the extraction system. Typical blank values in volts, during the course of these experiments, including 1σ errors are as follows: $^{35}Ar = (1.064 \pm 0.330) \times 10^{-8}$, $^{36}Ar = (1.521 \pm 0.004) \times 10^{-7}$, $^{37}Ar = (1.933 \pm 0.414) \times 10^{-8}$, $^{38}Ar = (2.849 \pm 1.156) \times 10^{-8}$, $^{39}Ar = (8.923 \pm 7.049) \times 10^{-10}$, and $^{40}Ar = (1.320 \pm 0.001) \times 10^{-5}$. For ^{40}Ar and ^{39}Ar, the blank seldom exceeded greater than 5 % of sample signal during the experiments. Air standards were analyzed before and after the sample analyses to determine the Ar sensitivity, as well as mass discrimination. The Ar sensitivity determined during the course of these experiments was 1.340×10^{11} V/mol. The mass discrimination correction factors for ^{36}Ar, ^{37}Ar, ^{38}Ar, and ^{39}Ar relative to ^{40}Ar were 0.973 ± 0.15 %, 0.981 ± 0.33 %, 0.987 ± 0.16 %, and 0.993 ± 0.57 %, respectively. Based on the present Ar sensitivity and low K content in the plagioclase-rich lithic fragments, individual fragments were outgassed in a single-step total fusion. Multiple step extraction would have resulted in the Ar signals below the present detection limit of the VG5400 mass spectrometer.

Sources of Ar in lunar regolith: radiogenic, cosmogenic, and trapped argon components

The top layer of lunar regolith is constantly bombarded by energetic particles originating from solar wind, solar cosmic rays, and galactic cosmic rays. The three stable isotopes of Ar (^{36}Ar, ^{38}Ar, and ^{40}Ar) are affected in different ways due to the interaction of lunar regolith with outer space. For example, ^{36}Ar resides close to the surface of individual grains and is mainly implanted by solar wind; this component is the trapped component (e.g., Wieler and Heber 2003). Cosmogenic ^{38}Ar is produced by interaction of energetic protons from solar and galactic cosmic rays with target elements such as Fe, Ca, K, and Ti. ^{40}Ar is produced by radioactive decay of ^{40}K; however, an "excess or parentless ^{40}Ar" component has also been observed in lunar regolith samples (Manka and Michel 1971). On the lunar surface, $^{40}Ar/^{36}Ar$ is 2–14 (e.g., Norman et al. 2003), and solar wind $^{40}Ar/^{36}Ar$ is 10^{-4} (Lodders 2010). The ^{40}Ar atoms present in the lunar atmosphere is photoionized and then accelerated by solar wind. About 50 % of the ^{40}Ar ions escape to space, and the remaining 50 % of ^{40}Ar atoms are driven back to the lunar surface (Signer et al. 1977). Only a few percent of ions are trapped in the lunar regolith while most ^{40}Ar ions are recycled to the lunar atmosphere. The small fraction of trapped lunar atmospheric ^{40}Ar has been proposed to be the source of excess ^{40}Ar in lunar regolith (e.g., Manka and Michel 1971; Wieler and Heber 2003). Below, we discuss procedures for calculating the abundance of radiogenic ^{40}Ar and cosmogenic ^{38}Ar to determine $^{40}Ar/^{39}Ar$ ages and ^{38}Ar cosmic ray exposure ages, respectively, for the plagioclase-rich lithic fragments.

Calculating the abundance of radiogenic ^{40}Ar

In the case of lunar regolith samples, the non-radiogenic ^{36}Ar originates from solar wind. Measured ^{40}Ar ($^{40}Ar_m$) is corrected for non-radiogenic ^{40}Ar using the non-radiogenic trapped $(^{40}Ar/^{36}Ar)_t$ and assuming the measured ^{36}Ar is of trapped Ar. Generally, a standard isochron plot ($^{40}Ar/^{36}Ar$ vs. $^{39}Ar/^{36}Ar$) is used where the *y*-intercept of a linear regression is assumed to be the trapped argon composition (e.g., Merrihue and Turner 1966; McDougall and Harrison 1999). We use two approaches to determine the trapped $^{40}Ar/^{36}Ar$ composition from total fusion analyses of plagioclase-rich lithic fragments. The first approach assumes that all the fragments contain the same trapped ($^{40}Ar/^{36}Ar$) composition. The second approach assumes that a trapped $^{40}Ar/^{36}Ar = 0$.

Calculating the abundance of cosmogenic ^{38}Ar

The measured ^{38}Ar abundances in the plagioclase-rich lithic fragments result from (1) nucleogenic (i.e., reactor produced), (2) trapped, and (3) cosmogenic components. During neutron irradiation, ^{38}Ar can be produced from Ca (i.e., $^{42}Ca(n, n\alpha)^{38}Ar$) and K (i.e., $^{39}K(n,d)^{38}Ar$). Based on CaF_2 crystals that were also irradiated with plagioclase-rich lithic fragments, the $(^{38}Ar/^{37}Ar)_{Ca}$ is $(4.50 \pm 0.02) \times 10^{-5}$, a negligible contribution to total ^{38}Ar. To estimate the ^{38}Ar produced from K, we determined $(^{38}Ar/^{39}Ar)_K = 0.0120 \pm 0.0002$, on $KSiO_3$ glasses irradiated with the plagioclase-rich lithic fragments. ^{38}Ar can also be produced during irradiation from reactions on Cl (i.e., $^{37}Cl(n, \gamma)^{38}Cl(\beta^-)^{38}Ar$). However, in lunar regolith, the amount of Cl is very low, averaging 20 ppm (e.g., Taylor and Hodges 1981). Because cadmium shielding was used during irradiation, ^{38}Ar produced from ^{37}Cl can be neglected.

The trapped ^{38}Ar in lunar surface samples results from solar wind implantation ($(^{38}Ar/^{36}Ar)_t = 0.188$; Eberhardt et al. (1972)). Following previous studies (e.g., Fernandes

et al. 2013), the cosmogenic ^{38}Ar ($^{38}Ar_c$) in individual plagioclase-rich lithic fragments was determined using the following equation:

$$^{38}Ar_c = {}^{38}Ar_m - {}^{36}Ar_m \times \left(^{38}Ar/^{36}Ar\right)_t - \left[^{39}Ar_K \times \left(^{38}Ar/^{39}Ar\right)_K\right], \quad (1)$$

where $^{39}Ar_K = {}^{39}Ar^* = {}^{39}Ar_m - {}^{37}Ar_m \times (^{39}Ar/^{37}Ar)_{Ca}$; $(^{39}Ar/^{37}Ar)_{Ca} = (7.57 \pm 0.34) \times 10^{-4}$; $(^{38}Ar/^{39}Ar)_K = 0.012 \pm 0.0002$; and c, m, and t subscripts denote cosmogenic, measured, trapped (i.e., solar wind), respectively; and K and Ca subscripts indicate reactor-produced components.

Results

Argon data for the plagioclase-rich lithic fragments, corrected for blank contribution, and reactor-produced interferences are given in Table 2.

Solar wind-implanted ^{36}Ar

On the lunar surface, solar wind is the most dominant source of ^{36}Ar (i.e., ions of ^{36}Ar directly implanted in lunar regolith). Since the implantation of solar wind is depth dependent and can penetrate only a few microns on the lunar surface, the variation in abundance of ^{36}Ar is a function of solar wind implantation duration and/or the depth at which fragments were exposed to solar wind. The measured ^{36}Ar abundance ($^{36}Ar_m$) in eleven plagioclase-rich lithic fragments, corrected for blank contribution and mass discrimination, varies from 0.41×10^{-6} cm^3 STP/g (i.e., Plag#23) to 4.1×10^{-6} cm^3 STP/g (i.e., Plag#10) (Table 2).

Argon isotopic composition

The comparison of $(^{40}Ar/^{36}Ar)_m$ and $(^{38}Ar/^{36}Ar)_m$ ratios for eleven plagioclase-rich lithic fragments, corrected for blank and mass discrimination, is shown in Fig. 2. Generally, $^{40}Ar/^{36}Ar$ values are explained as a result of the mixture between non-radiogenic trapped and radiogenic argon compositions. Non-radiogenic trapped argon on the lunar surface is mostly solar wind-implanted argon as discussed above. The $(^{40}Ar/^{36}Ar)_m$ varies from 0.62 (i.e., Plag#14) to 15.5 (i.e., Plag#23) with higher values suggesting the presence of radiogenic and/or excess parentless ^{40}Ar in the samples. The $(^{38}Ar/^{36}Ar)_m$ value for individual plagioclase-rich lithic fragments varies from ~0.191 to 0.6 (Fig. 2) and can be explained as a mixture of non-radiogenic trapped (i.e., $^{38}Ar/^{36}Ar = 0.188$; Eberhardt et al. (1972)) and cosmogenic Ar (i.e., $^{38}Ar/^{36}Ar = 1.54$; Hohenberg et al. (1978)). For the Plag#23 sample, the concentration of ^{36}Ar is lowest when compared to all other plagioclase-rich lithic fragments. We argue that the high $^{38}Ar/^{36}Ar$ ratio is a result of ^{36}Ar loss from Plag#23. The retentivity of noble gas components generally have an order: solar wind implanted (e.g., ^{36}Ar) <radiogenic (e.g., ^{40}Ar) <cosmogenic (e.g., ^{38}Ar). In general, solar wind-implanted gases are released at low temperature when stepwise heating is performed on lunar regolith samples (e.g., Hohenberg et al. 1970). This observation supports the argument that the solar wind-implanted Ar is more susceptible to loss compared to radiogenic and cosmogenic components of Ar.

$(^{40}Ar/^{36}Ar)_m$ vs. $(^{39}Ar/^{36}Ar)_m$ correlation

The $(^{40}Ar/^{36}Ar)_m$ and $(^{39}Ar/^{36}Ar)_m$ ratios were determined by correcting the measured abundances of ^{36}Ar, ^{40}Ar, and ^{39}Ar for blank contributions. In addition, the abundance of ^{36}Ar was corrected for mass discrimination, and the abundance of ^{39}Ar was corrected for radioactive decay since the time of sample irradiation. The $(^{40}Ar/^{36}Ar)_m$ and $(^{39}Ar/^{36}Ar)_m$ for eleven plagioclase-rich lithic fragments yield a strong linear correlation ($r^2 = 0.99$) (Fig. 3). Based on this linear regression, the $^{40}Ar/^{36}Ar$ intercept is 0.146 ± 0.002 and the slope is 335.44 ± 16.77. For the *x-y* error-weighted linear regression (York 1968), the intercept is 0.050 ± 0.104 and the slope is 336.49 ± 17.78. A linear correlation is generally observed in the case of isochron analysis of step heat experiments on undisturbed samples (e.g., Merrihue and Turner 1966; McDougall and Harrison 1999). A similar correlation is also observed for grain size fractions separated from regolith (e.g., Bogard and Nyquist 1975; Eberhardt et al. 1976), where the *y*-intercept represents the non-radiogenic composition of trapped $(^{40}Ar/^{36}Ar)_t$ and slope is used to determine the isochron age. Here, we discuss whether the apparent linear correlation observed in the case of the plagioclase-rich lithic fragments analyzed can be used to argue for the lithic fragments having (a) the same $^{40}Ar/^{39}Ar$ age and (b) the same $(^{40}Ar/^{36}Ar)_t$ (i.e., implanted solar wind).

$^{40}Ar/^{39}Ar$ ages

$^{40}Ar/^{39}Ar$ ages are calculated for the plagioclase-rich lithic fragments using three different approaches as described below. For all age determinations, a half-life of $1.250 \pm 0.002 \times 10^9$ for ^{40}K is used (Steiger and Jäger 1977; Renne et al. 2010).

Assuming the same trapped $(^{40}Ar/^{36}Ar)_t$ composition

In this first approach, we assume that all the plagioclase-rich lithic fragments contain the same trapped $(^{40}Ar/^{36}Ar)_t = 0.146$ (i.e., the *y*-intercept value on the $(^{40}Ar/^{36}Ar)_m$ versus $(^{39}Ar/^{36}Ar)_m$ regression (Fig. 3)). We prefer to use a slope obtained through normal regression as the correlation is observed for individual samples and

Table 2 Ar isotope data, cosmic ray exposure ages, $^{40}Ar/^{39}Ar$ ages for individual plagioclase-rich lithic fragments from Apollo 17, 78461 sample

Sample	$^{36}Ar_m$	$^{37}Ar_m$	$^{38}Ar_m$	$^{39}Ar_m$	$^{40}Ar_m$	$^{38}Ar_c$[a]	P_{38}^{sf}	P_{38}^{avg}	T_{38}^{sf}	T_{38}^{avg}	$^{40}Ar^*$	$^{40}Ar^*/^{39}Ar_K$	Age (Ga)	$^{40}Ar^*/^{39}Ar_K$	Age (Ga)
	(10^{-6} cm^3 STP/g)								(Ma)	(Ma)	(%)	$(^{40}Ar/^{36}Ar)_t = 0.146$		$(^{40}Ar/^{36}Ar)_t = 0.0$	
Plag#1	0.8598	2.0115	0.2047	0.0252	8.8056	4.28	0.77	0.17	5.55	25.21	99	367.44	4.27	372.69	4.30
	± 0.0015	± 0.0072	± 0.0004	± 0.0005	± 0.0044				± 0.83	3.78		6.24	± 0.05	6.25	± 0.04
Plag#3	1.0202	2.1366	0.3207	0.0140	4.6721	12.9	0.75	0.16	17.27	78.16	97	364.99	4.26	376.87	4.32
	0.0019	0.0095	0.0006	0.0003	0.0028				2.59	11.72		6.66	0.05	6.66	0.05
Plag#6	2.4610	1.5909	0.5121	0.0218	8.3324	4.92	0.73	0.16	6.75	30.69	96	388.51	4.37	405.82	4.44
	0.0044	0.0090	0.0013	0.0008	0.0050				1.01	4.60		13.89	0.07	14.87	0.07
Plag#9	1.7646	1.9960	0.4568	0.0285	10.7986	12.5	0.76	0.17	16.33	74.24	98	391.73	4.38	401.19	4.42
	0.0031	0.0072	0.0009	0.0004	0.0077				2.45	11.14		2.49	0.04	2.59	0.04
Plag#10	4.0690	1.9384	0.9513	0.0084	4.5744	18.6	0.77	0.17	24.20	109.47	87	578.00	5.03	663.19	5.26
	0.0072	0.0068	0.0021	0.0002	0.0030				3.63	16.42		17.89	0.06	18.30	0.06
Plag#14	3.4637	2.0183	0.7720	0.0069	2.1377	12.1	0.76	0.17	15.82	71.55	76	303.48	3.96	396.18	4.40
	0.0065	0.0074	0.0017	0.0001	0.0018				2.37	10.73		10.56	0.07	10.77	0.06
Plag#21	0.5082	1.2445	0.1361	0.0106	3.4686	4.04	0.76	0.17	5.34	24.18	98	353.29	4.21	360.92	4.25
	0.0008	0.0041	0.0002	0.0001	0.0011				0.80	3.63		1.20	0.04	1.31	0.04
Plag#22	1.0221	1.8797	0.2122	0.0119	3.5167	2.00	0.78	0.17	2.57	11.77	96	323.01	4.06	337.15	4.13
	0.0016	0.0063	0.0004	0.0001	0.0013				0.39	1.77		1.78	0.04	1.86	0.04
Plag#23	0.4147	1.6445	0.2482	0.0190	6.4346	17.0	0.79	0.17	21.53	97.48	99	359.57	4.24	362.95	4.25
	0.0007	0.0055	0.0004	0.0002	0.0012				3.23	14.62		1.45	0.04	1.58	0.04
Plag#24	0.9031	1.3672	0.1915	0.0284	9.5823	2.14	0.76	0.17	2.81	12.79	99	346.31	4.18	351.08	4.20
	0.0014	0.0048	0.0003	0.0003	0.0020				0.42	1.92		1.29	0.04	1.65	0.04
Plag#25	2.2802	1.6158	0.4375	0.0154	5.5328	0.87	0.78	0.17	1.11	5.05	94	369.07	4.28	392.43	4.38
	0.0037	0.0056	0.0008	0.0002	0.0017				0.17	0.73		2.12	0.04	2.40	0.04

The subscript m indicates that the measured abundance of Ar isotopes are corrected for blank contribution and mass discrimination. The subscript c indicates cosmogenic abundance determined by subtracting trapped component from the measured abundance of ^{38}Ar. Please see the text for details. $^{40}Ar^*/^{39}Ar_K$ and $^{40}Ar/^{39}Ar$ ages are given for two different methods (described in text) used for determining radiogenic ^{40}Ar in the fragments. To determine the ratio $^{40}Ar^*/^{39}Ar_K$, measured ^{40}Ar abundance is corrected for blank contribution, mass discrimination, and non-radiogenic trapped ^{40}Ar (i.e., solar wind-implanted ^{40}Ar) while measured ^{39}Ar is corrected for blank contribution, mass discrimination, and corrected for reactor-produced ^{39}Ar from ^{39}K. ^{38}Ar production rates are in units of 10^{-8} cm^3 STP/g/Ma

sf production rate calculated assuming lithic fragments were exposed to cosmic rays on lunar surface, *avg* production rate calculated based on average of production rates at the depth from 1 to 6 cm (corresponding shielding depth from 2 to 10 g/cm^2)

*Percentage of radiogenic component in measured ^{40}Ar when corrected for trapped contribution (i.e., $(^{40}Ar/^{36}Ar)_t = 0.146$)

[a]Units of (10^{-8} cm^3 STP/g)

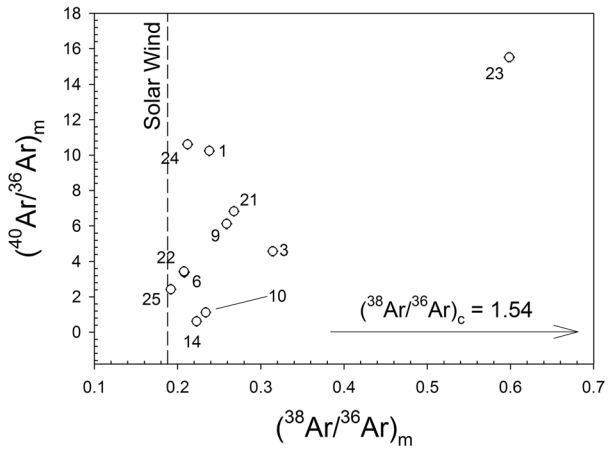

Fig. 2 Argon three isotope plot for plagioclase-rich lithic fragments. $(^{40}Ar/^{36}Ar)_m$ vs. $(^{38}Ar/^{36}Ar)_m$ for eleven plagioclase-rich lithic fragments separated from Apollo 17, 78461 regolith sample. The observed variation in $(^{38}Ar/^{36}Ar)$ values can be explained by mixing of non-radiogenic trapped Ar implanted via the solar wind (*vertical dashed line* $^{38}Ar/^{36}Ar = 0.188$ (Eberhardt et al. 1972)) and cosmogenic ($^{38}Ar/^{36}Ar = 1.54$ (Hohenberg et al. 1978)) ^{38}Ar in lunar plagioclase-rich lithic fragments. *m* = measured isotopic composition corrected for blank contribution and mass discrimination. The *numbers beside the symbols* represent the sample names (e.g., *10* represents sample Plag#10)

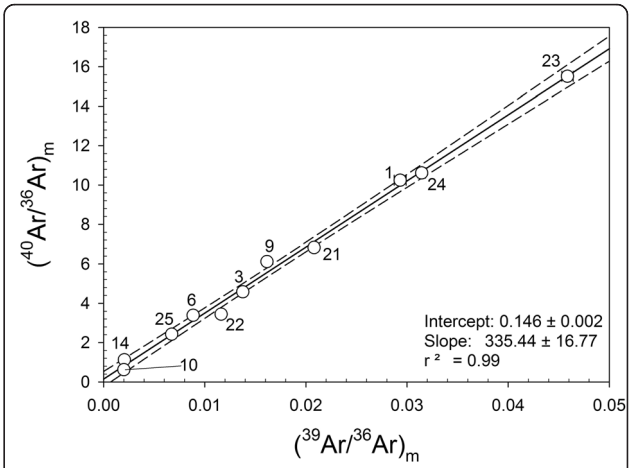

Fig. 3 The correlation between $^{40}Ar/^{36}Ar$ and $^{39}Ar/^{36}Ar$. Measured $^{40}Ar/^{36}Ar$ and $^{39}Ar/^{36}Ar$ for eleven plagioclase-rich lithic fragments separated from 78461 trench regolith sample. Plagioclase-rich lithic fragments show linear fit with a slope of ~335. The $^{40}Ar/^{39}Ar$ age estimated based on $^{40}Ar/^{39}Ar = 335.44$ is 4.33 ± 0.09 Ga. The *dashed lines* show 2σ deviations for the linear regression. $(^{40}Ar/^{36}Ar)_m$ and $(^{39}Ar/^{36}Ar)_m$ ratio were determined after correcting measured abundances of ^{36}Ar, ^{40}Ar, and ^{39}Ar for blank contribution. In addition, the abundance of ^{36}Ar was corrected for mass discrimination, and the abundance of ^{39}Ar was corrected for radioactive decay since the time of sample irradiation. The *numbers beside the symbols* represent the sample names (e.g., *10* represents sample Plag#10)

the correlation between errors of $^{39}Ar/^{36}Ar$ (*x*-axis) and $^{40}Ar/^{36}Ar$ (*y*-axis) is not expected unlike the case of an age isochron where *x*-*y* error-weighted linear regression is required. The $^{40}Ar/^{39}Ar$ ages determined by this approach range from 3.96 to 5.03 Ga. (Table 2, Fig. 4).

Assuming the absence of trapped ^{40}Ar

For this second approach, we assume that the plagioclase-rich lithic fragments are devoid of any trapped ^{40}Ar (i.e., $(^{40}Ar/^{36}Ar)_t = 0$). In this case, it is assumed that all the measured ^{40}Ar is radiogenic ^{40}Ar (e.g., Norman et al. 2006; Fernandes et al. 2013). The calculated $^{40}Ar/^{39}Ar$ ages determined in this way range from 4.13 to 5.26 Ga (Table 2, Fig. 4).

$^{40}Ar/^{39}Ar$ age based on $(^{40}Ar/^{36}Ar)_m$ vs. $(^{39}Ar/^{36}Ar)_m$ correlation

A third approach does not assume a trapped $(^{40}Ar/^{36}Ar)_t$ composition. As discussed in the "$(^{40}Ar/^{36}Ar)_m$ vs. $(^{39}Ar/^{36}Ar)_m$ correlation" section, we obtained a $^{40}Ar/^{39}Ar$ age of 4.13 ± 0.09 Ga for all the lithic fragments based on the slope of the linear regression (i.e., $^{40}Ar^*/^{39}Ar_K = 335.44 \pm 16.77$) observed on the correlation plot (Fig. 3). If we use the slope of linear regression (based on the York method), the $^{40}Ar/^{39}Ar$ age =4.135 ± 0.086 Ga, similar to the age derived using a slope obtained through linear regression. In Fig. 4, this age is compared with individual $^{40}Ar/^{39}Ar$ ages determined using the approaches outlined in the "Assuming the same trapped $(^{40}Ar/^{36}Ar)_t$ composition" and "Assuming the absence of trapped ^{40}Ar" sections above. The comparison of $^{40}Ar/^{39}Ar$ ages derived from three different approaches clearly indicate the sensitivity of age determination to the choice of trapped $(^{40}Ar/^{36}Ar)_t$.

CRE ages

On the lunar surface, ^{38}Ar is produced by solar as well as galactic cosmic rays. With the knowledge of ^{38}Ar production rate, it is possible to estimate the duration of cosmic ray exposure for individual plagioclase-rich lithic fragments. However, the production rate depends on the shielding depths. Hohenberg et al. (1978) calculated the production rates of ^{38}Ar on the lunar surface, as well as various shielding depths. These production rates are for 2π exposure geometry and give a production rate of ^{38}Ar, produced predominantly from the target element Ca, with smaller amounts contributed from Fe, Ti, and K. Assuming that the plagioclase-rich lithic fragments received the cosmic ray exposure on the lunar surface, we calculated production rates for ^{38}Ar using the measured major elemental compositions following surface production rates given by Hohenberg et al. (1978). These production rates are the maximum production rate estimates and range from 0.73 to 0.79×10^{-8} cm^3 STP g^{-1} Ma^{-1}. However, the depths from which the plagioclase-rich lithic fragments were sampled is not known precisely. As noted previously, the samples analyzed were picked

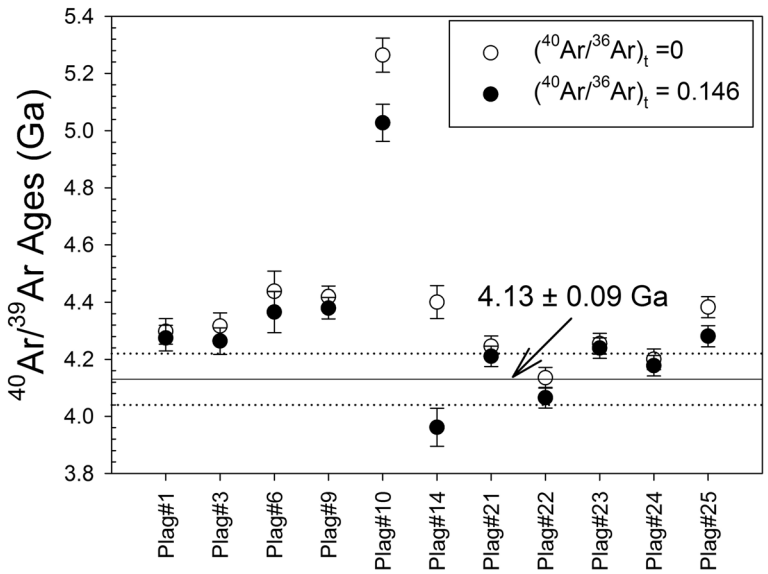

Fig. 4 $^{40}Ar/^{39}Ar$ ages of plagioclase-rich lithic fragments. $^{40}Ar/^{39}Ar$ ages of individual plagioclase-rich lithic fragments. The *filled symbols* represents the $^{40}Ar/^{39}Ar$ ages calculated after correcting measured ^{40}Ar for non-radiogenic trapped component using $(^{40}Ar/^{36}Ar)_t = 0.146$ (i.e., the *y*-intercept, Fig. 3). The *open symbols* represents $^{40}Ar/^{39}Ar$ ages calculated without any correction in measured ^{40}Ar for trapped contribution (e.g., Norman et al. 2006; Fernandes et al. 2013). The *horizontal line* represents the age of 4.13 ± 0.09 Ga, determined using the slope obtained in Fig. 3. The uncertainty shown for $^{40}Ar/^{39}Ar$ ages are 1σ

from ~410 g of regolith sampled from 1 to 6 cm depth. We calculated production rates using average production rates of 2, 5, and 10 g/cm^2 corresponding to 1.3, 3.3, and 6.6 cm depths, respectively (Hohenberg et al. 1978). The production rate for surface (P_{38}^{sf}) and average production rate for 1 to 6 cm depth (P_{38}^{avg}) along with respective ^{38}Ar cosmic ray exposure ages (T_{38}^{sf} and T_{38}^{avg}) are listed in Table 2 and plotted in Fig. 5. Because the abundance of the major target element (i.e., Ca) is similar for all the plagioclase-rich lithic fragments (Table 1), the range of the production rates is narrow as listed in Table 2. The surface exposure ages (T_{38}^{sf}) for plagioclase-rich lithic fragments vary from ~1 to 24 Ma representing the minimum exposure duration for the fragments. On the other hand, the exposure ages based on the average production rate for 1 to 6 cm depth (T_{38}^{avg}) range from ~5 to 110 Ma.

Interpretation of $^{40}Ar/^{39}Ar$ ages

Although the small sample weights (0.06–1.20 mg) precluded step heat experiments from being performed on the plagioclase-rich lithic fragments, the laser total fusion ages can be viewed as equivalent to total integrated ages based on step heat results (e.g., Lister and Baldwin 1996) assuming no loss or implantation of ^{40}Ar. The relatively tight clustering of inferred total fusion $^{40}Ar/^{39}Ar$ ages (i.e., 3.96 to 4.28 Ga) for eleven plagioclase-rich lithic fragments as well as older age range (~4 Ga) for the fragments indicate a modest disturbance among the entire set of samples with negligible loss of radiogenic ^{40}Ar. However, low temperature diffusive loss of Ar cannot be ruled out completely. Low temperature loss in the lunar samples have apparently occurred at a time closer to the formation ages. For example, Shuster et al. (2010) reported concordance in the initial step ages (ranging from 3.3–3.4 Ga) for 63503 samples which have different $^{40}Ar/^{39}Ar$ plateau ages and argued that the last significant loss of $^{40}Ar^*$ occurred 3.3–3.4 Ga ago. It should be noted that the initial step age provides an estimate for the timing associated with the last significant $^{40}Ar^*$ loss from a sample. Boehnke et al. (2015) also observed a broad peak at ~3.7 Ga for the Apollo 16 impact-melt samples based on initial minimum ages. This observation is inconsistent with the proposed late heavy bombardment (LHB) type event at ~3.85 Ga (e.g., Tera et al. 1974). Based on these observations, we argue that the lunar regolith most likely experienced impact events that peaked at ~3.7 Ga. Also, the loss of radiogenic ^{40}Ar at a younger time would result in greater difference between the total fusion age and the plateau age derived by step heat experiments. For example, the $^{40}Ar/^{39}Ar$ data reveal partial resetting resulting in ~29 % of ^{40}Ar loss at ~2.3 Ga for 77,017 samples (Hudgins et al. 2008). The total fusion age for 77017 is 3.741 ± 0.083 Ga while the plateau age is 4.018 ± 0.04 Ga, respectively. Similarly, the loss of around ~49 % ^{40}Ar at 3.2 Ga was estimated for sample 60035 (Hudgins et al. 2008) while the total fusion age is 4.088 ± 0.100 Ga. We infer that the difference between total fusion age and the plateau age is proportional to the (1) fraction of $^{40}Ar^*$ loss and

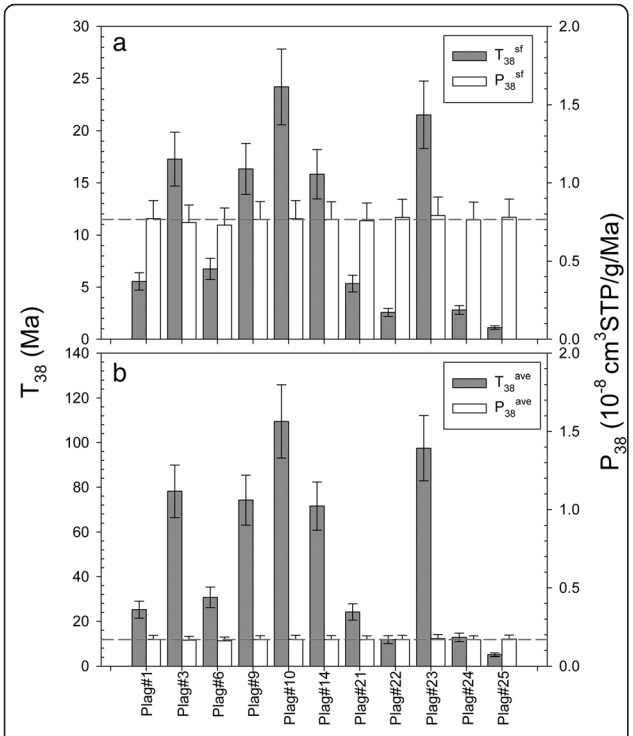

Fig. 5 The cosmic ray exposure ages along with ^{38}Ar production rates for plagioclase-rich lithic fragments. Cosmic ray exposure (CRE) ages (*left y*-axis) and ^{38}Ar production rates (*right y*-axis) for individual plagioclase-rich lithic fragments from 78461 regolith sample. The CRE ages and production rates are determined assuming that fragments were exposed either on lunar surface (i.e., T_{38}^{sf}, P_{38}^{sf}, **a**) or at depth between surface to 10 g/cm^2 (i.e., T_{38}^{avg}, P_{38}^{avg}, **b**). P_{38}^{avg} is the average of production rates at 2, 5, and 10 g/cm^2. The production rates are calculated using the major elemental compositions following production rates given by Hohenberg et al. (1978). Since plagioclase-rich lithic fragments have similar chemical compositions (as shown in Table 1), the production rates are also similar for the fragments. The variation in cosmic ray exposure ages is interpreted to result from the variation in abundances of cosmogenic ^{38}Ar. *Dashed line* indicates the average of ^{38}Ar production rates

(2) time difference between crystallization of sample and time of partial resetting. In the present study, we find total fusion ^{40}Ar/^{39}Ar ages from 3.96 to 4.28 Ga for eleven plagioclase-rich lithic fragments. Despite a tight clustering and older ^{40}Ar/^{39}Ar ages, we cannot rule out the possibility of partial resetting of ^{40}Ar/^{39}Ar ages in the plagioclase lithic fragments from regolith.

The two approaches used to determine the ^{40}Ar/^{39}Ar ages (sections "Assuming the same trapped $(^{40}Ar/^{36}Ar)_t$ composition" and "Assuming the absence of trapped ^{40}Ar") highlight the fact that the trapped non-radiogenic ^{40}Ar/^{36}Ar chosen for age calculation impacts the calculated ^{40}Ar/^{39}Ar ages (Fig. 4) of plagioclase-rich lithic fragments (c.f., Norman et al. (2003)). For example, Plag#14 has the lowest ^{40}Ar/^{39}Ar age (~3.96 Ga, Fig. 4), if measured ^{40}Ar is corrected using the trapped contribution ($(^{40}Ar/^{36}Ar)_t$ = 0.146), obtained from the *y*-intercept on the $(^{40}Ar/^{36}Ar)_m$ vs. $(^{39}Ar/^{36}Ar)_m$ diagram. In comparison, the age of Plag#14 is similar to that of other fragments (Fig. 4) when we assume $(^{40}Ar/^{36}Ar)_t = 0$. On the contrary, the ^{40}Ar/^{39}Ar age for Plag#10 is ~5.0 Ga (assuming $(^{40}Ar/^{36}Ar)_t = 0.146$) and ~5.3 Ga (assuming $(^{40}Ar/^{36}Ar)_t = 0$), and both approaches yielded geologically meaningless ages.

Both these plagioclase-rich lithic fragments (i.e., Plag#10 and Plag#14) have the lowest $(^{40}Ar/^{36}Ar)_m$ and $(^{39}Ar/^{36}Ar)_m$ (Fig. 3). Assuming non-radiogenic trapped $(^{40}Ar/^{36}Ar)_t = 0.143$, the percentage of radiogenic ^{40}Ar (^{40}Ar*) released from Plag#10 and Plag#14 is approximately 87 and 76 %, respectively, while the rest of the samples yielded >94 % ^{40}Ar* (Table 2). Plag#10 and Plag#14 have higher $^{36}Ar_m$ compared to that of other fragments; however, the ^{40}Ar/^{39}Ar ages do not appear to be a function of the abundance of measured ^{36}Ar (Fig. 6). As we have assumed the same value of non-radiogenic trapped ^{40}Ar/^{36}Ar (i.e., 0.143), the correction for trapped contribution in measured ^{40}Ar is higher for Plag#10 and Plag#14, owing to their higher abundance of ^{36}Ar. Overcorrection for $(^{40}Ar)_m$ could explain the lowest ^{40}Ar/^{39}Ar age for Plag#14 (i.e., 3.96 Ga). It is possible that Plag#14 fragment may have a lower or no trapped $(^{40}Ar/^{36}Ar)_t$ component. On the other hand, the highest apparent ^{40}Ar/^{39}Ar age for Plag#10 can be due to the higher amount of non-radiogenic trapped ^{40}Ar/^{36}Ar. The $^{40}Ar^*/^{39}Ar_K$ ratio for the Plag#10 fragment is the highest (i.e., ~578) when compared to that of other plagioclase-rich lithic fragments including Plag#14 (ranging from 303 to 391) (Table 2). We conclude that Plag#10 sample contains parentless ^{40}Ar. This can explain the geologically meaningless apparent age (i.e., an age of a sample cannot be older than the age of solar system). The Plag#10 fragment also has the highest CRE age (i.e., 24 to 110 Ma, depending on the choice of production rate; Table 2), indicating longer residence on the lunar surface. We propose that during residence on the lunar surface, ^{40}Ar that was present in the lunar atmosphere was ionized and implanted in the Plag#10 fragment by solar wind, resulting in entrapment of excess or parentless ^{40}Ar.

Results yielded total fusion ^{40}Ar/^{39}Ar ages that are interpreted as minimum crystallization ages of the plagioclase-rich lithic fragments. If samples have been partially outgassed due to heating following crystallization (e.g., due to impacts on lunar surface), this would result in loss of radiogenic ^{40}Ar from the lithic fragments, therefore lowering the ^{40}Ar/^{39}Ar ages. On the other hand, implantation of unknown amount of parentless ^{40}Ar from lunar atmosphere through SW would result in higher ^{40}Ar/^{39}Ar ages. Therefore, it is difficult to characterize the amount of loss of ^{40}Ar and/or implantation of ^{40}Ar in single-millimeter fragments. Although we were unable to resolve possible details of the thermal history following crystallization, results are comparable to an integrated ^{40}Ar/^{39}Ar age for

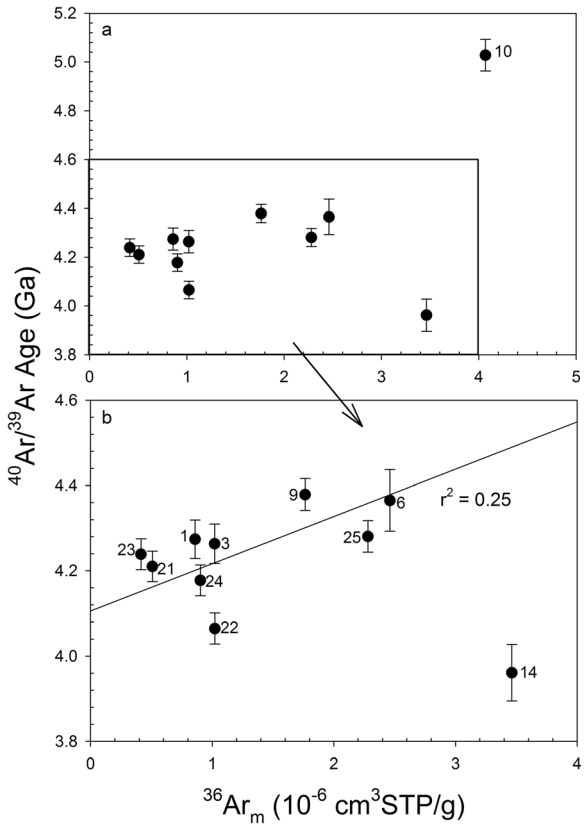

Fig. 6 No correlation exists between ^{36}Ar concentration and $^{40}Ar/^{39}Ar$ ages of plagioclase-rich lithic fragments. **a** $^{40}Ar/^{39}Ar$ ages of individual plagioclase-rich lithic fragments compared with the abundance of ^{36}Ar. **b** Comparison excluding the Plag#10 fragment. A poor correlation is observed between the ages and ^{36}Ar abundances of the fragments. The $^{40}Ar/^{39}Ar$ ages are determined after correcting measured ^{40}Ar for non-radiogenic trapped contribution. The *numbers beside the symbols* represent the sample names (e.g., *10* represents sample Plag#10)

step heat experiments, assuming no loss of ^{40}Ar or implantation of ^{40}Ar, and thus provide minimum ages of crystallization (e.g., Lister and Baldwin 1996). However, it is highly possible that lunar regolith could have experienced complicated history of ^{40}Ar degassing and implantation as discussed below.

Discussion

During the early lunar evolution (>4 Ga), a greater amount of ^{40}K was available to decay to ^{40}Ar in the lunar crust and this radiogenic ^{40}Ar escaped to lunar atmosphere (e.g., Eugster et al. 2001). A fraction of the escaped ^{40}Ar was ionized and accelerated by solar wind. Eventually, a small fraction of ^{40}Ar (5–8.5 %; Manka and Michel 1971) was implanted by the solar wind into the lunar surface. The $^{40}Ar/^{36}Ar$ ratio of trapped Ar in lunar regolith has decreased throughout lunar history, roughly in phase with the decreasing ^{40}K; however, the initial $^{40}Ar/^{36}Ar$ composition of argon trapped in the regolith is uncertain and dependent on the ambient environment at the time of crystallization. This is especially relevant if impact ejecta are the source of regolith. On the other hand, the lunar regolith experiences gardening processes and impact events by micrometeorites that may have a variable effect dependent on regolith size. For example, grains that spent more time on the lunar surface are susceptible to impacts by micrometeorites unlike grains at a few centimeters depth. The gardening process can randomly excavate small grains multiple times. These processes affect the lunar regolith and therefore the trapped $^{40}Ar/^{36}Ar$ composition of regolith material.

What is the trapped non-radiogenic $^{40}Ar/^{36}Ar$ composition in lunar regolith?

The selection of trapped non-radiogenic $^{40}Ar/^{36}Ar$ is critical for the determination of $^{40}Ar/^{39}Ar$ ages. However, in the case of total fusion experiments and step heat experiments where isochron plot does not yield a meaningful *y*-intercept (i.e., 67215 clast; Norman et al. 2003), it is difficult to determine the trapped non-radiogenic $^{40}Ar/^{36}Ar$ composition. For lunar regolith, the trapped $^{40}Ar/^{36}Ar$ composition has a range of values. For example, orange glass from 74001/2 core drilled near the Shorty crater at the Apollo 17 landing site has $^{40}Ar/^{36}Ar$ composition ranging from 8 to 10 (Eugster et al. 1980). Two Apollo 14 breccia samples (14301 and 14318) have trapped $^{40}Ar/^{36}Ar$ composition ranging between 10 and 14 (Megrue 1973; Reynolds et al. 1974; Bernatowicz et al. 1980). $^{40}Ar/^{36}Ar$ values for breccia samples from Apollo 16 regolith lie in the range of <1 to 12 (McKay et al. 1986). In the present study, the measured $^{40}Ar/^{36}Ar$ ratio in plagioclase-rich lithic fragments ranges from 0.62 to 15.5, which is similar to the ratios reported.

Comparison of results with previously reported isochron ages

The $^{40}Ar/^{39}Ar$ total fusion ages determined for the lithic fragments are the first ages ever determined for the trench soil collected at station 8 using any isotopic study. However, an approximately 0.5-m-diameter boulder also collected at station 8 (~50 m from the trench, Fig. 1), at the base of the Sculptured Hills, has been extensively studied. Jackson et al. (1975) concluded that the coarse-grained, cumulus-textured boulder formed at a depth of 8–30 km in the lunar crust and was excavated by a large basin-forming impact event. The boulder originated via impact generated ballistic transport to the present site and cannot be related to the geology of the Apollo 17 landing area or the Sculptured Hills. Samples 78235, 78236, 78238, 78255, and 78256 are derived from the same boulder. Figure 7 gives the compilation of ages derived by various isotopic dating methods. The ages range from 4.00 ± 0.09 Ga

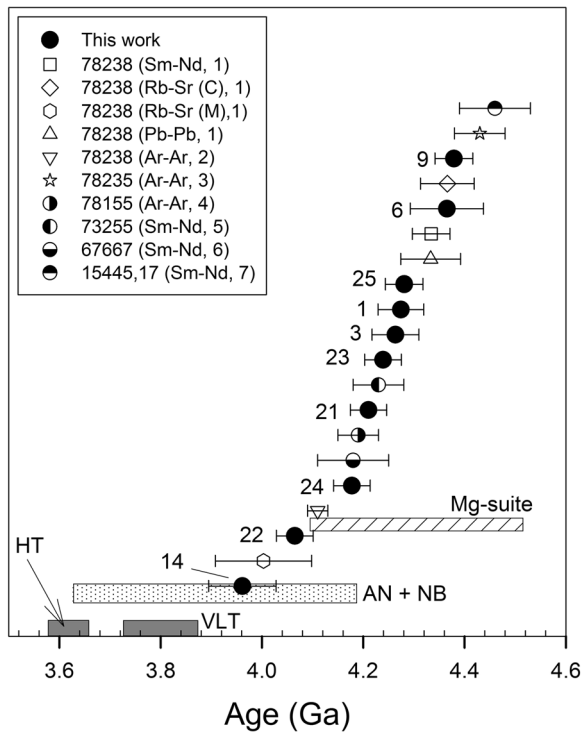

Fig. 7 Comparison of $^{40}Ar/^{39}Ar$ ages of plagioclase-rich lithic fragments with other studies of relevant lunar rocks. Ages for rocks from station 8, Apollo 17, and Mg-suite highland rocks compared with the plagioclase-rich lithic fragments. The *numbers beside the symbols* represent the sample names (e.g., *14* represents sample Plag#14). Data from: *1* Edmunson et al. (2009); *2* Aeschilimann et al. (1982); *3* Nyquist et al. (1981); *4* Fernandes et al. (2013); *5* Carlson and Lugmair (1981a); *6* Carlson and Lugmair (1981b); *7* Shih et al. (1993)

(metamorphic age for 78238 using Rb-Sr study (Edmunson et al. 2009) to ~4.43 ± 0.05 Ga (crystallization age based on Sm-Nd for most retentive phases (Nyquist et al. 1981)). The Rb-Sr metamorphic age is concordant with an $^{40}Ar/^{39}Ar$ age of 4.11 ± 0.02 for 78235/78236 (Aeschlimann et al. 1982). As can be seen in Fig. 7, the $^{40}Ar/^{39}Ar$ total fusion ages of plagioclase-rich lithic fragments (except Plag#10) fall within the age range observed for the station 8 boulder 78238. However, it should be noted that there is no apparent genetic relation between the lithic fragments and the boulder based on the origin of the boulder 78238 inferred by Jackson et al. (1975).

The crystallization ages of Mg-suite rock samples are also compared with the $^{40}Ar/^{39}Ar$ ages of the plagioclase-rich lithic fragments (Fig. 7). Sample 78155, also collected at station 8 (~20 m from the trench at the rim of Bowen-Apollo crater, Fig. 1), a thermally annealed polymict breccia of anorthositic norite composition (Bickel 1977), has a $^{40}Ar/^{39}Ar$ crystallization age of 4.19 ± 0.04 Ga (Fernandes et al. 2013), within the range observed for the plagioclase-rich lithic fragments reported here (Fig. 7). Delano and Bence (1977) reported two ~4-mm plagioclase-rich lithic fragments belonging to the Mg-suite that had been collected ~5 km from station 8 (station 3; regolith 73260) at the Apollo 17 site. These two lithic fragments, both belonging to the Mg-suite, had $^{40}Ar/^{39}Ar$ ages of ~4.2 Ga obtained by stepwise heating. A comparison of $^{40}Ar/^{39}Ar$ ages of plagioclase-rich lithic fragments with the crystallization age ranges observed for other lithologic components reveal that the lithic fragments overlap the age range observed for polymict breccia (anorthositic norite and noritic) and Mg-suite rocks, suggesting these lithologic components as possible origins for the lithic fragments as discussed in "Origin of the plagioclase-rich fragments" section below.

Implications for lunar surface processes based on CRE ages

The CRE ages of the lithic fragments represent integrated durations of exposure on the surface of the Moon and reveal an exposure and a burial history of the regolith samples. The variation in CRE ages (from ~1 to 24 Ma (based on ^{38}Ar production rate for surface exposure) or ~5 to 110 Ma (based on average ^{38}Ar production rate for 1 to 6 cm depth on lunar surface) indicates that individual plagioclase-rich lithic fragments have not remained stationary and instead have experienced movement within the lunar regolith for durations of 1 Ma. On the Moon, regolith from a depth of 9 mm is thought to overturn at least once in approximately 10 Ma (Hörz et al. 1991). The estimated CRE range, determined for the plagioclase-rich lithic fragments is consistent with previous suggested regolith overturn rates. The CRE ages for rock samples also collected at station 8 sample range from 17 to 292 Ma (Drozd et al. 1977; Hudgins et al. 2008; Fernandes et al. 2013). The CRE ages observed for some plagioclase-rich lithic fragments are similar to previously reported CRE age of ~17 to 21 Ma for the 78155 samples (Hudgins et al. 2008; Fernandes et al. 2013). Trench regolith from station 8 contained mature samples based on carbon content and maturity index (McKay et al. 1974). The deepest sample from trench (78421) is a mature regolith containing a high abundance of agglutinates (68 %). Based on the low albedo data (Apollo Lunar Geology Investigation Team 1973) and inferred regolith maturity on the basis of fossil track data (Goswami and Lal 1974), it was argued that a large fraction of the regolith at the Apollo 17 site was exposed and reworked at the lunar surface for significant periods of time. Since the plagioclase-rich lithic fragments were derived from the regolith at the base of Sculptured Hills, it is possible that the regolith at station 8 may have been affected by downslope movement of materials from higher elevations. The observed range for CRE ages, either ~1 to 24 Ma or ~5 to 110 Ma, for eleven plagioclase-rich lithic fragments suggests that there is a heterogeneous distribution of submillimeter-sized fragments with a range of cosmic ray exposure ages in the top layer of lunar regolith at station 8.

Table 3 Lithologic components that contributed to the trench regolith sample collected at station 8, Apollo 17

Lithologic components	Age (Ga)	Proportions at station 8 (%)	Modal percent plagioclase	Plagioclase composition	Fe/(Fe + Mg) in plagioclase
Mare basalt (92 % high-Ti and 8 % very-low-Ti basalts)					
High-Ti (HT)	3.75 ± 0.01 to 3.85 ± 0.04 (1)	25.8	23 (7)	An_{86}-An_{87} (8)	0.38 to 0.62 (8)
Very-low-Ti (VLT)	3.63 ± 0.04 (2)	2.2	32 (7)	An_{93}-An_{96} (8)	0.65 to 0.84 (8)
Orange glass (OG)	3.60 ± 0.04 (3) to 3.66 ± 0.04 (4)	12.0	–	–	
Highland rocks					
Anorthositic norite (AN)	3.75 ± 0.11 to 4.16 ± 0.04 (1)	35.7	60–80 (9)	An_{85}-An_{98} (9)	0.44 to 1.00 (9)
Noritic breccia (NB)		15.7	40–60 (9)	An_{86}-An_{98} (9)	0.19 to 1.00 (9)
Mg-suite (60 % troctolite and 40 % norite)					
Mg-suite troctolite (Mg-T)	4.46 ± 0.07 (5) to 4.18 ± 0.07 (6)	4.62	60-85(10)	An_{94}-An_{97} (11)	0.44 to 1.00 (11)
Mg-suite norite (Mg-N)		3.08	40-70(10)	An_{93}-An_{94} (11)	0.31 to 0.54 (11)

Modified after Table 5 of Korotev and Kremser (1992). Data sources are given in parentheses: (1) Tables 5.7 and 5.8 of Stöffler et al. (2006), (2) Zellner et al. (2009), (3) Huneke and Wasserburg (1978), (4) Alexander et al. (1980), (5) Shih et al. (1993), (6) Carlson and Lugmair (1981a), (7) Papike and Vaniman (1978), (8) Table 5.5 of Papike et al. (1991), (9) Table 5.6 and Figure 5.8 of Papike et al. (1991), (10) Table 3 of Wieczorek et al. (2006), (11) Table 5.7 of Papike et al. (1991)

Origin of the plagioclase-rich fragments

The lunar regolith generally spans a large range of chemical compositions and the variations result from different proportions of major lithologic components that originate from mare basalt and highland rocks. Korotev and Kremster (1992) presented a mass-balance model to account for the compositional variation observed in the regolith samples collected during the Apollo 17 mission. Korotev and Kremster (1992) concluded that various proportions of three chemical components of mare origin (high-Ti and very-low-Ti basalts, pyrocloastic orange glass) and three components of highland origin (impact-melt noritic breccia, anorthositic norite breccia, Mg-suite) can account for most of the compositional variation observed for Apollo 17 regolith. A mixing model, based on major and trace-element compositions, reveals that the trench regolith sample collected at station 8 contains 25.8 % of HT basalt, 2.2 % of VLT basalt, 12 % of orange glass, 15.7 % of impact-melt NB, 35.7 % of AN breccia, 4.62 % of troctolite Mg-suite, and 3.1 % of norite Mg-suite (Table 3, Korotev and Kremser 1992). With the exception of orange glass, these components contain different proportions of plagioclase grains (Table 3). We use mole percent anorthite (i.e., $CaAl_2Si_2O_8$) and Fe/(Fe + Mg) in plagioclase-rich lithic fragments to further constrain the origin of the lithic fragments. In Fig. 8, we compare An(%) and Fe/(Fe + Mg) values of plagioclase-rich lithic fragments (Table 1) with that of possible protoliths listed in Table 3. Based on this comparison, we conclude that none of the plagioclase-rich lithic fragments are inferred to be derived from HT mare basalt (Fig. 8a). This comparison also suggests multiple possible origins for a given plagioclase-rich lithic fragments due to overlapping values of An(%) and Fe/(Fe + Mg) for the lithologic components. We observe that the An(%) and Fe/(Fe + Mg) values of the Plag#1 lithic fragment do not

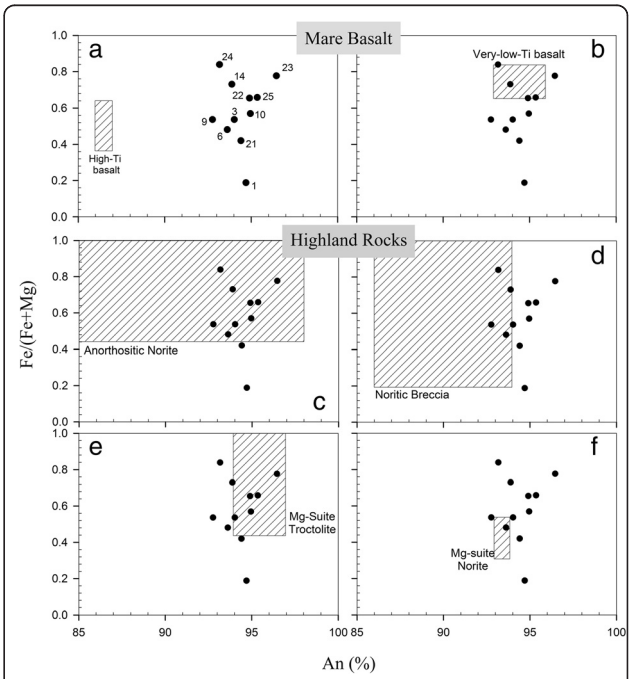

Fig. 8 Comparison of Fe/(Fe + Mg) and An(%) for plagioclase-rich lithic fragments with lunar lithologies. Fe/(Fe + Mg) and An(%) for plagioclase-rich lithic fragments (*filled circles*) compared with mare basalt and highland rocks. The *hatched area* in all the panels represent the range of values (Table 3) observed for different lithologic components. **a** *Numbers beside the circles* represent sample names (e.g., *1* Plag#1). No lithic fragments overlap the range of values reported for high-Ti basalt. **b** Plag#24, Plag#14, Plag#22, and Plag#25 have compositions similar to VLT basalt. **c** Except Plag#1, all the lithic fragments overlap the range of composition observed for AN component. **d** Plag#24, Plag#14, Plag#3, Plag#9, and Plag#8 have compositions similar to that of NB component. **e** The compositions of Plag#23, Plag#22, Plag#25, Plag#10, Plag#3, and Plag#21 are within the range observed for troctolite component of Mg-suite rocks. **f** Three plagioclase-rich lithic fragments (i.e., Plag#3, Plag#6, and Plag#9) have compositions within the range observed for the norite component of Mg-suite rocks. Source of data for different lithologic compositions is given in Table 3

overlap with that of any lithologic component. However, impact-melt NB could possibly contribute Plag#1 fragment. At least four lithic fragments may have originated from very-low-Ti mare basalt, while most of the plagioclase-rich lithic fragments may have originated from the highland region. We further constrain the lithologic origin of the plagioclase-rich lithic fragments based on the range of crystallization ages reported for different lithologic components (Table 3). The crystallization ages for highland polymict rocks (i.e., AN and NB) range from 3.75 ± 0.11 Ga to 4.16 ± 0.04 Ga (Stöffler et al. 2006). These overlaps with the younger age range are obtained for the plagioclase-rich lithic fragments (Fig. 7). Based on crystallization ages, it can also be argued that no lithic fragment originated from the VLT mare basalt, and most of the fragments may have been derived from the Mg-suite rocks. Simon et al. (1981) observed that mare volcanics and highland-derived fragments were present in similar proportions in Apollo 17 regolith sample 78221, the deepest part of the trench regolith collected at station 8. Similarly, mixing models based on major and trace-element composition indicate that the top layer of trench regolith at the station 8 (i.e., 78481) is composed of 40–50 % of mare and 52–59 % of highlands (Rhodes et al. 1974; Korotev and Kremser 1992). A recent study suggests that pure anorthosite is widely distributed over the entire Moon (Nagaoka et al. 2014). Contrary to thier suggestion, our results indicate that the fragments collected at the base of the Sculptured Hills are mostly derived from the Mg-suite rocks. However, it should be noted that the plagioclase-rich fragments analyzed in this work were selectively sampled and therefore should not be expected to yield similar results to previous studies based on bulk compositional data (Rhodes et al. 1974; Simon et al. 1981; Korotev and Kremser 1992). Due to the known lithologic complexity of the Sculptured Hills (Robinson and Jolliff 2002), and the plagioclase-rich fragments targeted for analysis, it is not surprising that the eleven plagioclase-rich lithic fragments were strongly biased against mare basaltic fragments.

Conclusions

We present the first $^{40}Ar/^{39}Ar$ ages on plagioclase-rich lithic fragments separated from trench regolith collected at station 8 during the Apollo 17 mission. The apparent $^{40}Ar/^{39}Ar$ ages for plagioclase-rich lithic fragments in general range from 4.0 to 4.4 Ga assuming a trapped $^{40}Ar/^{36}Ar$ of 0.146 (Fig. 3), the *y*-intercept of the regression between $(^{40}Ar/^{36}Ar)_m$ and $(^{39}Ar/^{36}Ar)_m$. One sample (Plag#10) contains excess ^{40}Ar interpreted to result from implantation of parentless ^{40}Ar together with solar wind while exposed on the lunar surface. The CRE duration of Plag#10 is the longest among all the grains analyzed suggesting that this grain likely spent a longer duration on the lunar surface, most likely before 4 Ga and hence higher ^{40}Ar was likely implanted with the solar wind. The variation in CRE ages (from ~1 to 24 Ma) in plagioclase-rich lithic fragments indicates that individual fragments have experienced recent movement within the lunar regolith during this time likely due to downslope movement at the base of the Sculptured Hills. Based on the chemical mixing model Korotev and Kremser (1992), chemical compositions, and $^{40}Ar/^{39}Ar$ ages, we argue that most of the plagioclase-rich lithic fragments analyzed in this study originated from Mg-suite of highland rocks. No plagioclase-rich fragments were derived from the mare region. The chemical and argon isotopic records preserved in Apollo 17 station 8 plagioclase-rich lithic fragments illustrate the wealth of information obtainable from submillimeter-sized samples returned from planetary objects including the Moon, Mars, and asteroids.

Abbreviations

AN: anorthositic norite; CLICIT: cadmium-lined in-core irradiation tube; CRE: cosmic ray exposure; HT: high-titanium mare basalt; NB: noritic breccia; VLT: very-low-Ti basalt.

Competing interests

The authors declare that they have no competing interests.

Authors' contributions

SLB and JD conceived the project. JD separated the lithic fragments and characterized them. JPD designed and performed the experiments in consultation with SLB. JPD wrote the manuscript, together with SLB and JD. All authors read and approved the final manuscript.

Acknowledgements

This study was conducted in collaboration with the New York Center for Astrobiology. Financial support was provided by the NASA Astrobiology Institute (grant NNA09DA80A). We thank E. B. Watson for discussions during the course of this project. We thank Mark Norman for his constructive comments on an earlier draft of the manuscript. Jisun Park and an anonymous reviewer are thanked for their constructive comments that helped further improve the manuscript.

Author details

[1]Department of Earth Sciences, Syracuse University, Syracuse, NY 13244, USA. [2]Department of Atmospheric and Environmental Sciences, University of Albany (SUNY), Albany, NY 12222, USA.

Received: 14 July 2015 Accepted: 23 January 2016
Published online: 26 January 2016

References

Aeschlimann U, Eberhardt P, Geiss J, Grogler N, Kurtz J, Marti K (1982) On the age of cumulate norite 78236: an 39AR-40AR study. Proc Lunar Planet Sci 13:1–2

Alexander EC Jr, Coscio MR Jr, Dragon JC, Saito K (1980) K/Ar dating of lunar soils. IV—orange glass from 74220 and agglutinates from 14259 and 14163. Proc Lunar Planet Sci 11:1663–77

Team ALGI (1973) Preliminary geologic analysis of the Apollo 17 site. US Geological Survey

Bernatowicz TJ, Hohenberg CM, Hudson B, Kennedy BM, Podosek FA, Laul JC (1980) Noble gas component organization in 14301. Proc Lunar Planet Sci 11:629–68

Bickel CE (1977) Petrology of 78155—an early, thermally metamorphosed polymict breccia. Proc Lunar Planet Sci 2:2007–27

Boehnke P, Heizler MT, Harrison TM, Lovera OM. Warren PH. (2015) Lunar 40Ar/39Ar Data Does Not Indicate a ca. 3.9 Ga Impact Episode. In: Lunar and Planetary Institute Science Conference Abstracts. p 2745.

Bogard DD, Nyquist LE (1973) $^{40}Ar/^{36}Ar$ variations in Apollo 15 and 16 regolith. Proc Lunar Planet Sci 2:1975–1985
Butler P (1973) Lunar sample information catalog, Apollo 17: Houston. Lunar Receiving Lab., Lyndon B. Johnson Space Center, p 99.
Carlson RW, Lugmair GW (1981a) Time and duration of lunar highlands crust formation. Earth Planet Sci Lett 52:227–38. doi:10.1016/0012-821X(81)90177-1
Carlson RW, Lugmair GW (1981b) Sm-Nd age of lherzolite 67667: implications for the processes involved in lunar crustal formation. Earth Planet Sci Lett 56:1–8. doi:10.1016/0012-821X(81)90112-6
Delano JW, Bence AE (1977) 4.2-4.3 AE anorthositic soil fragments—equilibrated or unequilibrated polycomponent systems. Proc Lunar Planet Sci 8:2029–50
Drozd RJ, Hohenberg CM, Morgan CJ, Podosek FA, Wroge ML (1977) Cosmic-ray exposure history at Taurus-Littrow. Proc Lunar Planet Sci 8:3027–43
Eberhardt P, Eugster O, Geiss J, Groegler N, Guggisberg S, Moergeli M (1976) Noble gases in the Apollo 16 special soils from the East–west split and the permanently shadowed area. Proc Lunar Planet Sci 7:563–85
Eberhardt P, Geiss J, Graf H, Gr6gler N, Mendia MD, M6rgeli M, Schwaller H and Stettler A. (1972) Trapped solar wind noble gases in Apollo 12 lunar fines 12001 and Apollo 11 breccia 10046. In: Lunar and Planetary Science Conference Proceedings. pp 1821–1856.
Edmunson J, Borg LE, Nyquist LE, Asmerom Y (2009) A combined Sm–Nd, Rb–Sr, and U–Pb isotopic study of Mg-suite norite 78238: further evidence for early differentiation of the moon. Geochim Cosmochim Acta 73:514–27. doi:10.1016/j.gca.2008.10.021
Eugster O, Groegler N, Eberhardt P, Geiss J (1980) Double drive tube 74001/2—composition of noble gases trapped 3.7 AE ago. Proc Lunar Planet Sci 11:1565–92
Eugster O, Terribilini D, Polnau E, Kramers J (2001) The antiquity indicator argon-40/argon-36 for lunar surface samples calibrated by uranium-235-xenon-136 dating. Meteorit Planet Ldots 115:1097–115
Fernandes VA, Fritz J, Weiss BP, Garrick-Bethell I, Shuster DL (2013) The bombardment history of the moon as recorded by 40 Ar- 39 Ar chronology. Meteorit Planet Sci 48:241–69. doi:10.1111/maps.12054
Gombosi DJ, Baldwin SL, Watson EB, Swindle TD, Delano JW, Roberge WG (2015) Argon diffusion in Apollo 16 impact glass spherules: implications for 40Ar/39Ar dating of lunar impact events. Geochim Cosmochim Acta 148:251–68. doi:10.1016/j.gca.2014.09.031
Goswami JN, Lal D (1974) Cosmic ray irradiation pattern at the Apollo 17 site—implications to lunar regolith dynamics. Proc Lunar Planet Sci 5:2643–62
Graf JC (1993) Lunar soils grain size catalog. NASA reference publication. 1256: p 436.
Grotzinger JP, Crisp J, Vasavada AR, Anderson RC, Baker CJ, Barry R, Blake DF, Conrad P, Edgett KS, Ferdowsi B, Gellert R, Gilbert JB, Golombek M, Gomez-Elvira J, Hassler DM, Jandura L, Litvak M, Mahaffy P, Maki J, Meyer M, Malin MC, Mitrofanov I, Simmonds JJ, Vaniman D, Welch RV, Wiens RC (2012) Mars science laboratory mission and science investigation. Space Sci Rev 170:5–56. doi:10.1007/s11214-012-9892-2
Heiken G, McKay DS (1974) Petrography of Apollo 17 soils. Proc Lunar Planet Sci 1:843–60
Hohenberg CM, Davis PK, Kaiser WA, Lewis RS, Reynolds JH (1970) Trapped and cosmogenic rare gases from stepwise heating of Apollo 11 samples. Geochim Cosmochim Acta Suppl 1:1283
Hohenberg CM, Marti K, Podosek FA, Reedy RC, Shirck JR (1978) Comparisons between observed and predicted cosmogenic noble gases in lunar samples. Proc Lunar Planet Sci 9:2311–44
Hörz F, Grieve R, Heiken G, Spudis P, Binder A (1991) Lunar surface processes. Lunar Sourceb User's Guide Moon 61–120.
Hudgins JA, Spray JG, Kelley SP, Korotev RL, Sherlock SC (2008) A laser probe 40Ar/39Ar and INAA investigation of four Apollo granulitic breccias. Geochim Cosmochim Acta 72:5781–98. doi:10.1016/j.gca.2008.08.024
Huneke JC, Wasserburg GJ (1978) 40AR-39AR ages of single orange glass balls and highland breccia phenocrysts. Proc Lunar Planet Sci 9:567–9
Jackson ED, Sutton RL, Wilshire HG (1975) Structure and petrology of a cumulus norite boulder sampled by Apollo 17 in Taurus-Littrow Valley, the moon. Geol Soc Am Bull 86:433–42. doi:10.1130/0016-7606(1975)86<433:SAPOAC>2.0.CO;2
Jourdan F, Renne PR (2007) Age calibration of the Fish Canyon sanidine 40Ar/39Ar dating standard using primary K–Ar standards. Geochim Cosmochim Acta 71:387–402. doi:10.1016/j.gca.2006.09.002
Korotev RL, Kremser DT (1992) Compositional variations in Apollo 17 soils and their relationship to the geology of the Taurus-Littrow site. Proc Lunar Planet Sci 22:275–301
Kring DA (2015) Human and Robotic Missions: To the Moon Again and Beyond. Eos. doi: 10.1029/2015EO024609.
Lauretta DS, Team O-R (2012) An Overview of the OSIRIS-REx Asteroid Sample Return Mission. In: Lunar and Planetary Institute Science Conference Abstracts. p 2491.
Lister GS, Baldwin SL (1996) Modelling the effect of arbitrary P-T-t histories on argon diffusion in minerals using the MacArgon program for the Apple Macintosh. Tectonophysics 253:83–109. doi:10.1016/0040-1951(95)00059-3
Lodders K (2010) Solar system abundances of the elements. In: Goswami A, Reddy BE (eds) Principles and perspectives in cosmochemistry. Springer, Berlin Heidelberg, pp 379–417
Lucey P, Korotev RL, Gillis JJ, Taylor LA, Lawrence D, Campbell BA, Elphic R, Feldman B, Hood LL, Hunten D, Mendillo M, Noble S, Papike JJ, Reedy RC, Lawson S, Prettyman T, Gasnault O, Maurice S (2006) Understanding the lunar surface and space-moon interactions. Rev Mineral Geochem 60:83–219. doi:10.2138/rmg.2006.60.2
Manka RH, Michel FC (1971) Lunar atmosphere as a source of lunar surface elements. Proc Lunar Planet Sci 2:1717
McDougall I, Harrison TM (1999) Geochronology and Thermochronology by the 40Ar/39Ar Method. Oxford University Press, USA.
McKay DS, Bogard DD, Morris RV, Korotev RL, Johnson P, Wentworth SJ (1986) Apollo 16 regolith breccias: characterization and evidence for early formation in the mega-regolith. Proc Lunar Planet Sci 16:277
McKay DS, Fruland RM, Heiken GH (1974) Grain size distribution as an indicator of the maturity of lunar soils. Lunar Science Conference, In, pp 480–2
Megrue GH (1973) Spatial distribution of 40Ar/39Ar ages in lunar breccia 14301. J Geophys Res 78:3216–21. doi:10.1029/JB078i017p03216
Merrihue C, Turner G (1966) Potassium-argon dating by activation with fast neutrons. J Geophys Res 71:2852–7. doi:10.1029/JZ071i011p02852
Meyer C (2010) The lunar sample compendium. http://curator.jsc.nasa.gov/lunar/lsc/index.cfm.
Mitchell JK, Carrier WD III, Costes NC, Houston WN, Scott RF, Hovland HJ (1973) Soil Mechanics. p 8.
Nagaoka H, Takeda H, Karouji Y et al (2014) Implications for the origins of pure anorthosites found in the feldspathic lunar meteorites, Dhofar 489 group. Earth Planets Space 66:115. doi:10.1186/1880-5981-66-115
Norman MD, Borg LE, Nyquist LE, Bogard DD (2003) Chronology, geochemistry, and petrology of a ferroan noritic anorthosite clast from Descartes breccia 67215: Clues to the age, origin, structure, and impact history of the lunar crust. Meteorit Planet Sci 38:645–61. doi:10.1111/j.1945-5100.2003.tb00031.x
Norman MD, Duncan RA, Huard JJ (2006) Identifying impact events within the lunar cataclysm from 40Ar–39Ar ages and compositions of Apollo 16 impact melt rocks. Geochim Cosmochim Acta 70:6032–49. doi:10.1016/j.gca.2006.05.021
Nyquist LE, Bogard DD, Wooden JL, Bansal BM, Wiesmann H, Shih C-Y (1981) A comparative Rb-Sr, Sm-Nd, and K-Ar study of shocked norite 78236—evidence of slow cooling in the lunar crust. Proc Lunar Planet Sci 13:67–97
Okada T, Zolensky ME, Ireland TR, Yada T (2015) The Earth, Planets and Space special issue: "science of solar system materials examined from Hayabusa and future missions". Earth Planets Space 67:116. doi:10.1186/s40623-015-0235-x
Papike JJ, Vaniman DT (1978) Luna 24 ferrobasalts and the mare basalt suite - Comparative chemistry, mineralogy, and petrology. In Mare Crisium: The view from Luna 24, edited by Merrill R. B. and Papike J. J. New York: Pergamon Press. p 371–401.
Papike J, Taylor L, Simon S (1991) Lunar minerals. In: Lunar sourcebook: a user's guide to moon. University Press, Cambridge, pp 121–81
Renne PR, Mundil R, Balco G, Min K, Ludwig KR (2010) Joint determination of 40 K decay constants and 40Ar /40 K for the Fish Canyon sanidine standard, and improved accuracy for 40Ar/39Ar geochronology. Geochim Cosmochim Acta 74:5349–67. doi:10.1016/j.gca.2010.06.017
Reynolds JH, Alexander EC Jr, Davis PK, Srinivasan B (1974) Studies of K-Ar dating and xenon from extinct radioactivities in breccia 14318; implications for early lunar history. Geochim Cosmochim Acta 38:401–17. doi:10.1016/0016-7037(74)90134-3
Rhodes JM, Rodgers KV, Bansal BM, Wiesmann H, Shih C, Nyquist LE, Hubbard NJ (1974) The relationships between geology and soil chemistry at the Apollo 17 landing site. Proc Lunar Planet Sci 5:1097–117
Robinson MS, Jolliff BL (2002) Apollo 17 landing site: topography, photometric corrections, and heterogeneity of the surrounding highland massifs. J Geophys Res Planets 107:5110. doi:10.1029/2001JE001614

Schwarz W, Trieloff M (2007) Intercalibration of 40Ar–39Ar age standards NL-25, HB3gr hornblende, GA1550, SB-3, HD-B1 biotite and BMus/2 muscovite. Chem Geol 242:218–31. doi:10.1016/j.chemgeo.2007.03.016
Shih C-Y, Nyquist LE, Dasch EJ, Bogard DD, Bansal BM, Wiesmann H (1993) Ages of pristine noritic clasts from lunar breccias 15445 and 15455. Geochim Cosmochim Acta 57:915–31. doi:10.1016/0016-7037(93)90178-Y
Shuster DL, Balco G, Cassata WS, Fernandes VA, Garrick-Bethell I, Weiss BP (2010) A record of impacts preserved in the lunar regolith. Earth Planet Sci Lett 290: 155–65. doi:10.1016/j.epsl.2009.12.016
Signer P, Baur H, Etique P, Frick U, Funk H (1977) On the question of the 40Ar excess in lunar soils. Philos Trans R Soc Lond Ser Math Phys Sci 285:385–90
Simon SB, Papike JJ, Laul JC (1981) The lunar regolith—comparative studies of the Apollo and Luna sites. Petrology of soils from Apollo 17, Luna 16, 20, and 24. Proc Lunar Planet Sci 12:371–88
Steiger RH, Jäger E (1977) Subcommission on geochronology: convention on the use of decay constants in geo- and cosmochronology. Earth Planet Sci Lett 36:359–62. doi:10.1016/0012-821X(77)90060-7
Stöffler D, Ryder G, Ivanov BA, Artemieva NA, Cintala MJ, Grieve RAF (2006) Cratering history and lunar chronology. Rev Mineral Geochem 60:519–96. doi:10.2138/rmg.2006.60.05
Taylor SR, Hodges RR (1981) Chlorine and sulfur abundances in mars and the moon: implications for bulk composition. Proc Lunar Planet Sci 12:1082–4
Tera F, Papanastassiou DA, Wasserburg GJ (1974) Isotopic evidence for a terminal lunar cataclysm. Earth Planet Sci Lett 22:1–21. doi:10.1016/0012-821X(74)90059-4
Tsuda Y, Yoshikawa M, Abe M, Minamino H, Nakazawa S (2013) System design of the Hayabusa 2—asteroid sample return mission to 1999 JU3. Acta Astronaut 91:356–62. doi:10.1016/j.actaastro.2013.06.028
Turner G (1971) Argon 40-argon 39 dating: the optimization of irradiation parameters. Earth Planet Sci Lett 10:227–34. doi:10.1016/0012-821X(71)90010-0
Wieczorek MA, Jolliff BL, Khan A, Pritchard ME, Weiss BP, Williams JG, Hood LL, Righter K, Neal CR, Shearer CK, McCallum IS, Tompkins S, Hawke BR, Peterson C, Gillis JJ, Bussey B (2006) The constitution and structure of the lunar interior. Rev Mineral Geochem 60:221–364. doi:10.2138/rmg.2006.60.3
Wieler R, Heber VS (2003) Noble gas isotopes on the moon. Space Sci Rev 106: 197–210. doi:10.1023/A:1024641805441
Wolfe EW, Bailey NG, Lucchitta BK, Muehlberger WR, Scott DH, Sutton RL, Wilshire HG, Batson RM, Larson KB, Tyner RL (1981) The geologic investigation of the Taurus-Littrow valley, Apollo 17 landing site. USGS Prof Pap 1080:280
York D (1968) Least squares fitting of a straight line with correlated errors. Earth Planet Sci Lett 5:320–4. doi:10.1016/S0012-821X(68)80059-7
Zellner NEB, Delano JW, Swindle TD, Barra F, Olsen E, Whittet DCB (2009) Apollo 17 regolith, 71501,262: a record of impact events and mare volcanism in lunar glasses. Meteorit Planet Sci 44:839–51. doi:10.1111/j.1945-5100.2009.tb00772.x